Ozone Profile Retrievals From the Cross-Track Infrared Sounder

Pengfei Ma, Liangfu Chen, Zhongting Wang, Shaohua Zhao, Qing Li, Minghui Tao, and Zifeng Wang

***Abstract*—This paper presents an algorithm for the retrieval of ozone profiles from the Cross-track Infrared Sounder (CrIS) aboard the Suomi National Polar-orbiting Partnership satellite using a nonlinear optimal estimation method. The issue of channel selection is discussed. Based on a sensitivity analysis, we selected a spectral range of 990–1070 cm^{-1} for the ozone profile retrievals. Compared with ERA-Interim ozone profiles and eigenvector regression method profiles, the ozone climatology profile is better able to construct the *a priori* state. The retrieved CrIS profiles are in good agreement with smoothed high-vertical-resolution ozonesonde profiles. An analysis of the information content of the CrIS retrievals demonstrates that the CrIS measurements can provide useful information for capturing the spatial and temporal variations in ozone and are insensitive to ozone below 400 hPa. An error analysis revealed that smoothing error represents the main error source for the retrieved CrIS ozone profiles.**

***Index Terms*—Cross-track Infrared Sounder (CrIS), eigenvector regression, nonlinear optimal estimation, ozone profile.**

I. Introduction

OZONE is a particularly critical trace gas in the Earth's atmosphere, because this molecule plays a key role in atmospheric photochemical reactions and in climate change. On average, approximately 90% of the atmospheric ozone is found in the stratosphere, and 10% is found in the troposphere [20]. Ozone in the stratosphere forms a protective shield that reduces the intensity of ultraviolet (UV) radiation from the sun at the Earth's surface and further determines the vertical profile of temperature. In the troposphere, where it is an important greenhouse gas, ozone traps heat in the Earth's atmosphere [17]. Because of its high reactivity, ozone is an extremely powerful oxidizing agent that damages rubber and plastics and is harmful to humans and plants even at low concentrations [37]. Monitoring globally distributed vertical ozone profiles is essential for understanding physical and chemical processes in the atmosphere, tracking stratospheric ozone depletion and tropospheric pollution, improving forecasts of the UV index, and estimating climate forcing from ozone [21]. Thus, ozone needs to be monitored with good spatial and temporal coverage.

Ozonesondes can provide ozone concentrations from the ground to approximately 30–35 km, with a very high vertical resolution (0.1 km), a precision better than $\pm$(3–5)%, and an accuracy of approximately $\pm$(5–10)% up to an altitude of 30 km [34]. However, spatial coverage is too sparse to provide a global picture of ozone distribution.

In recent decades, space-based remote sensing has been used to obtain dense spatial and temporal ozone measurements. The two major types of measurements with high spectral resolution are UV-visible and thermal infrared (TIR). UV measurements have been made by the Solar Backscatter Ultraviolet 2 (SBUV/2) instrument, which continues the NASA Nimbus-7 SBUV record that began in 1978 [12], [16], the Total Ozone Mapping Spectrometer (TOMS) series of instruments, which began operation with the Nimbus-7 TOMS in 1978 [24], [25], the Global Ozone Monitoring Experiment 2 (GOME-2) instrument, which continues the GOME instrument [2], the SCanning Imaging Absorption spectroMeter for Atmospheric CHartographY [2], the Ozone Monitoring Instrument (aboard Aura) [39], and the Ozone Mapping and Profiler Suite [aboard the Suomi National Polar-orbiting Partnership (Suomi NPP) satellite] [13]. High-resolution thermal infrared measurements have been made by the Interferometric Monitor for Greenhouse Gases (aboard ADEOS) [8], the Atmospheric Infrared Sounder (aboard AQUA) [10], the Tropospheric Emission Spectrometer (aboard EOS-AURA) [29], [38], the Infrared Atmospheric Sounding Interferometer (aboard MetOp-A) [3], [7], and the Cross-track Infrared Sounder (CrIS, aboard Suomi NPP). Both types of satellite-based observations can capture ozone variability and are weakly sensitive to the lowermost tropospheric ozone content. In the UV, the measurement sensitivity to the lowermost troposphere is low because of the Rayleigh backscatter of the incoming solar radiation as the air density increases in the lower troposphere, whereas in the TIR, measurement sensitivity to the lowermost troposphere requires high thermal contrast between the Earth's surface and the near-surface (tens to hundreds of meters above surface) atmosphere. However, TIR measurements will always provide information in the free troposphere in cloud-free conditions [30].

In this paper, we present a detailed study on the development of an algorithm for retrieving ozone profiles from the CrIS.

Manuscript received July 17, 2014; revised July 23, 2015 and December 14, 2015; accepted January 28, 2016. Date of publication March 28, 2016; date of current version May 24, 2016. This work was supported in part by the National Natural Science Foundation of China under Grant 41501407 and in part by the Environmental Protection Public Welfare Project under Grant 201309011. *(Corresponding author: Qing Li.)*

P. Ma, Z. Wang, S. Zhao, and Q. Li are with the Environmental Satellite Application Center and the State Environmental Protection Key Laboratory of Satellite Remote Sensing, Ministry of Environmental Protection, Beijing 100101, China (e-mail: mpf136@163.com; yzh_4_2002@sina.com; zshyytt@126.com; li.qing@mep.gov.cn).

L. Chen is with the State Key Laboratory of Remote Sensing Science, Institute of Remote Sensing and Digital Earth, Chinese Academy of Sciences, Beijing 100101, China (e-mail: lfchen@radi.ac.cn).

M. Tao and Z. Wang are with the State Key Laboratory of Remote Sensing Science, Institute of Remote Sensing and Digital Earth, Chinese Academy of Sciences, Beijing 100101, China (e-mail: taomh@radi.ac.cn; wangzf@radi.ac.cn).

Color versions of one or more of the figures in this paper are available online at http://ieeexplore.ieee.org.

Digital Object Identifier 10.1109/TGRS.2016.2532353

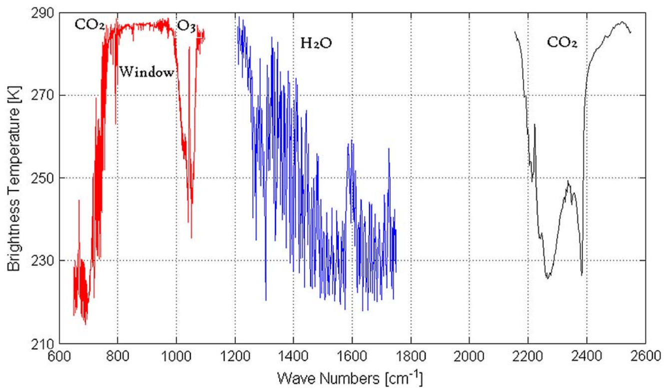

Fig. 1. CrIS observations above the Broadmeadows (March 3, 2012) site.

This study is important for us to improve the accuracy of ozone satellite remote sensing retrievals in future studies. The CrIS instrument is described in the next section. Section III explains the retrieval method and the characterization and error analysis. In Section IV, results from the different comparisons are shown and discussed. Finally, this paper is summarized in Section V.

II. CrIS Instrument

The CrIS, which is a Fourier transform spectrometer, was designed to produce high-resolution 3-D temperature, pressure, and moisture profiles to enhance weather forecast models for both short-term and long-term weather forecasting. Over longer timescales, these measurements will help improve our understanding of climate phenomena (http://npp.gsfc.nasa.gov/cris.html). The CrIS, which is aboard NASA's Suomi NPP satellite, was launched on October 28, 2011. It provides soundings of the atmosphere via 1305 spectral channels over three wavelength ranges: Long-wavelength infrared (LWIR) (9.14–15.38 μm), Mid-wavelength infrared (MWIR) (5.71–8.26 μm), and Short-wavelength infrared (SWIR) (3.92–4.64 μm), with unapodized spectral resolutions of 0.625, 1.25, and 2.5 cm$-$1, respectively. The CrIS swath is 2200 km wide with 30 fields-of-regard (FORs) per scan line. Each FOR contains nine fields of view, each of which has a 14-km diameter at nadir (see Fig. 2) [14]. Fig. 1 shows the measured CrIS brightness temperature spectra (see Fig. 2 for the CrIS footprint).

III. Inverse Method Description

A. Forward Model

For any remote measurement, the measured quantity y is some vector valued function f of the unknown state vector x and other parameters b that have an impact on the measurement [32]. The general forward model can be written as

$$Y = F(X, b) + \varepsilon. \tag{1}$$

In this paper, the state vector X is the ozone profile that will be retrieved, ε is the measurement noise, and F is the forward model. The vector b consists of surface parameters (emissivity and temperature) and atmospheric parameters (e.g., atmospheric profiles and clouds). In this paper, the k-matrix model of the Community Radiative Transfer Model (CRTM) [15] is used to simulate the CrIS radiances and their derivatives to the surface/atmospheric parameters in the retrieval state.

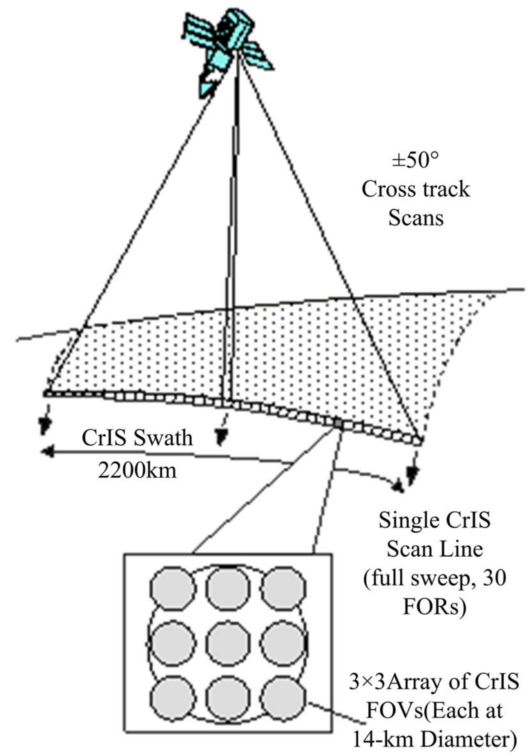

Fig. 2. CrIS footprint.

B. Retrieval Method

Our retrieval algorithm combines previous knowledge of the atmospheric state and new information obtained from measured spectral radiances. Because the retrieval problem is ill posed and has no unique and stable solution, regularization techniques must be utilized to find the best representation of the true state [22]. In this paper, we used an optimal estimation method to derive ozone profiles.

1) Optimal Estimation Method: The retrieval $\hat{x}$ is the result of the retrieval method R, and the scheme has been described in detail [32], i.e.,

$$\hat{x} = R\left(F(x, b) + \varepsilon, \hat{b}, x_a, S_a\right) \tag{2}$$

where x_a is an *a priori* profile (in this study, the *a priori* ozone profile is obtained using an eigenvector regression technique; see Section III-B2), $\hat{b}$ is the best estimate of the forward function parameter b, and S_a is the *a priori* covariance matrix. Since the forward model is usually a nonlinear function of the atmospheric state vector, an iterative method is needed to find the minimum of the cost function J, i.e.,

$$\begin{aligned} J = &(X - X_a)^T \cdot S_a^{-1} \cdot (X - X_a) \\ &+ (F(X) - Y)^T \cdot S_e^{-1} \cdot (F(X) - Y). \end{aligned} \tag{3}$$

The differences between the measured (Y) and simulated $(F(X))$ radiances and between the retrieved (X) and *a priori* (x_a) state vectors, constrained with the measurement error covariance matrix (S_e) and the *a priori* covariance matrix (S_a), are calculated in each iteration with the solution

$$\begin{aligned} X_{i+1} = X_a + &\left(K_i^T S_e^{-1} K_i + S_a^{-1}\right)^{-1} K_i^T S_e^{-1} \\ &\cdot [(Y - F(X_i)) - K_i(X_a - X_i)] \end{aligned} \tag{4}$$

where X_{i+1} and X_i are the current and previous state vectors, respectively. In our retrieval scheme, the first guess X_0 is chosen equal to the *a priori* profile X_a. $K = \partial Y / \partial X$, which is the weighting function, or the Jacobian matrix. The following *a priori* covariance matrix was used (see [32] and [18]):

$$(S_a)_{ij} = (\sigma_{x_a})_{ij}^2 \exp\left(-\frac{i-j}{h}\right) \qquad (5)$$

where $(\sigma_{x_a})_{ij}$ is the standard deviation of the climatology, and h is the length scale. The measurement error covariance matrix S_e is a diagonal matrix; the nondiagonal elements are set to zero.

Retrievals were only performed for cloud-free scenes, which were identified using a basic cloud filtering system based on the brightness temperatures at 11 and 12 μm and on their comparison with the European Centre for Medium-Range Weather Forecasts (ECMWF) analyses of the surface skin temperature [3]. The surface emissivity used over land is provided by an emissivity database [5], and the sea surface emissivity model is the Nalli model [28]. The temperature and water vapor profiles used in the inversion process are bilinear interpolations of the ECMWF temperature and specific humidity fields on the CrIS observation pixels. The state vector in the iterative retrieval includes only ozone profiles.

2) A Priori Profile: For ill-posed problems, other information in addition to the measurements is needed to constrain the solution and to choose a reasonable profile from the infinite number of mathematically possible profiles [11]. In the optimal estimation retrieval technique, this information generally takes the form of *a priori* profile, which is regarded as a very important prior restriction in order to obtain a stabilized and regularized solution [6], [23]. We evaluated three possible alternative *a priori* profiles, namely, the ECMWF profiles, the regression algorithm results, and the ozone climatology, and then chose a more accurate profile as the first guess profile.

ERA-Interim is the latest global atmospheric reanalysis produced by the ECMWF, for the period after January 1, 1989. It is a 12-h 4D-Var assimilation system, which assimilates TOMS total ozone, SBUV and SBUV/2 (on NOAA-14) ozone profiles, and GOME ozone profiles that are produced by the Rutherford Appleton Laboratory [9]. We used the ozone data on a horizontal grid of 1° in latitude by 1° in longitude with 37 pressure levels between the surface and 0.1 hPa.

The regression method provides a stable retrieval with a finer grid from 0.005 to 1100 hPa. In the regression algorithm, the channel radiances are first simulated for the global profiles of temperature, moisture, and ozone and surface temperatures from the SeeBorV5.0 profile database [1], which consists of 15 704 global profiles of temperature, moisture, and ozone at 101 pressure levels (between 1100 and 0.005 hPa) for clear-sky conditions. Using the simulated radiances y (we selected the first 1245 channels), the inverse solution can be written [35], [36] as

$$x = C \cdot y \qquad (6)$$

where the vector x contains the atmospheric profiles of the temperature, water vapor, and ozone. C is the best fit operator matrix obtained using a linear least square method, i.e.,

$$C = XY^T (YY^T + EE^T)^{-1} \qquad (7)$$

where (YY^T) is the covariance of the simulated radiance, (XY^T) is the covariance of the training profile with the simulated radiance, and (EE^T) is a statistical covariance of spectral radiance noise.

The ozone climatology that consists of monthly average ozone profiles for 10° latitude zones covering altitudes from 0 to 65 km was taken from [26] and is based on data from the Aura Microwave Limb Sounder (MLS; 2004–2010) and balloon sondes (1988–2010). The MLS instrument on Aura has much better latitude coverage than the SAGE II data that have been previously used and measures ozone daily from the upper troposphere to the lower mesosphere. The additional balloon data provided a much more accurate tropospheric ozone climatology [27].

We compare the ECMWF, regression, and climatological profiles with the ozonesonde data in Fig. 3. The colors of the profiles are as follows: regression in blue, ECMWF in green, climatology in red, and interpolated sonde in black. The colors of the relative differences are as follows: (regression–sonde)/sonde in blue, (climatology–sonde)/sonde in red, and (ECMWF–sonde)/sonde in green. All of the data were interpolated to the regression pressure grid. The comparison indicates that both the ECMWF and regression profiles are in good agreement with the sondes in the stratosphere, but are in relatively poor agreement in the troposphere, particularly at the bottom of the troposphere. In contrast, the ozone climatology provides a much more accurate tropospheric profile in most cases, particularly in the Southern Hemisphere. We therefore used the ozone climatology as the *a priori* profile.

3) Channel Selection: Ozone has an absorption band in the TIR spectrum at 9.6 μm, and we used the CrIS LWIR (650–1095 cm^{-1}) spectrum for the perturbation testing. We evaluated the brightness temperature (BT) response to the perturbation of each atmospheric constituent separately: 1 K for temperature (T), 10% for humidity (q), 10% for ozone (O_3), and 10% for carbon dioxide (CO_2). We perturbed these quantities at all the grid levels, and all the perturbations are positive. The brightness temperature response ΔBT is represented by the difference between the CRTM simulation with the perturbed profile and the reference profile. These BT differences indicate the sensitivity of each channel to each specific atmospheric species. Fig. 4 shows a plot of the differences. After this preliminary screening, we closely study the ozone weighting functions associated with the selected channels. Since the weighting function is the derivative of the transmittance profile, it will peak higher in the atmosphere for the frequency at which the absorption is stronger; one-peaked channels and the channels with the sharpest weighting functions are selected. Based on this, we selected the spectral region 990–1070 cm^{-1} for the ozone profile retrieval. Fig. 5 shows the absolute values of the ozone Jacobian matrix at selected channels for a tropical air mass (reference profile).

4) Retrieval Characterization and Inversion Error Analysis: The characterization and error analysis of profiles that are retrieved via remote sensing of the atmosphere are important for evaluating retrieval algorithms and the design of sounding systems and for guiding their calibration [31]. The retrieval sensitivity is characterized by the averaging kernel (AK) matrix A,

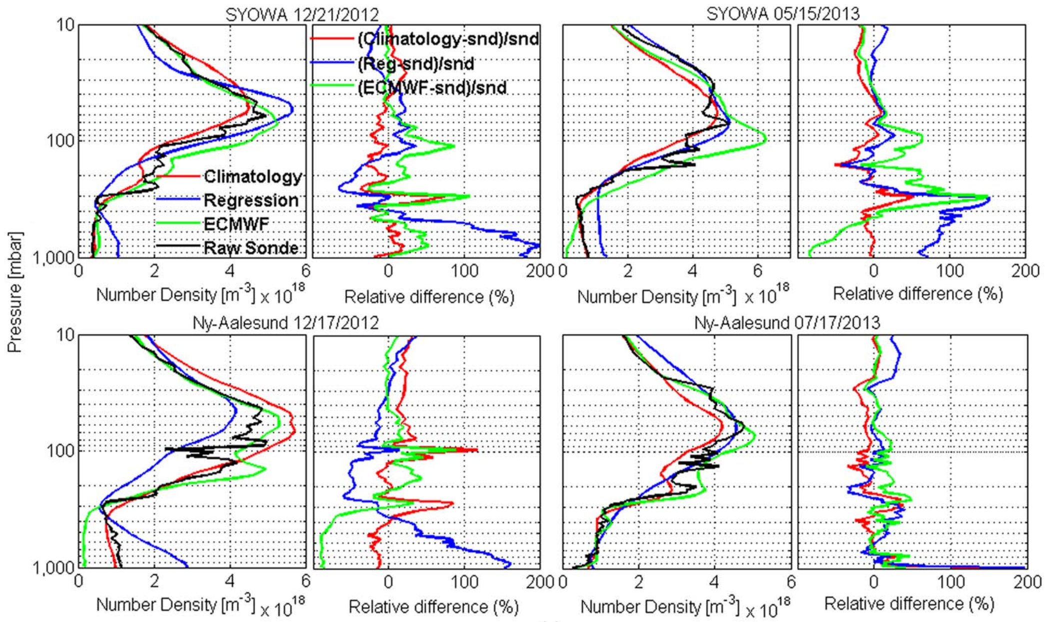

(a)

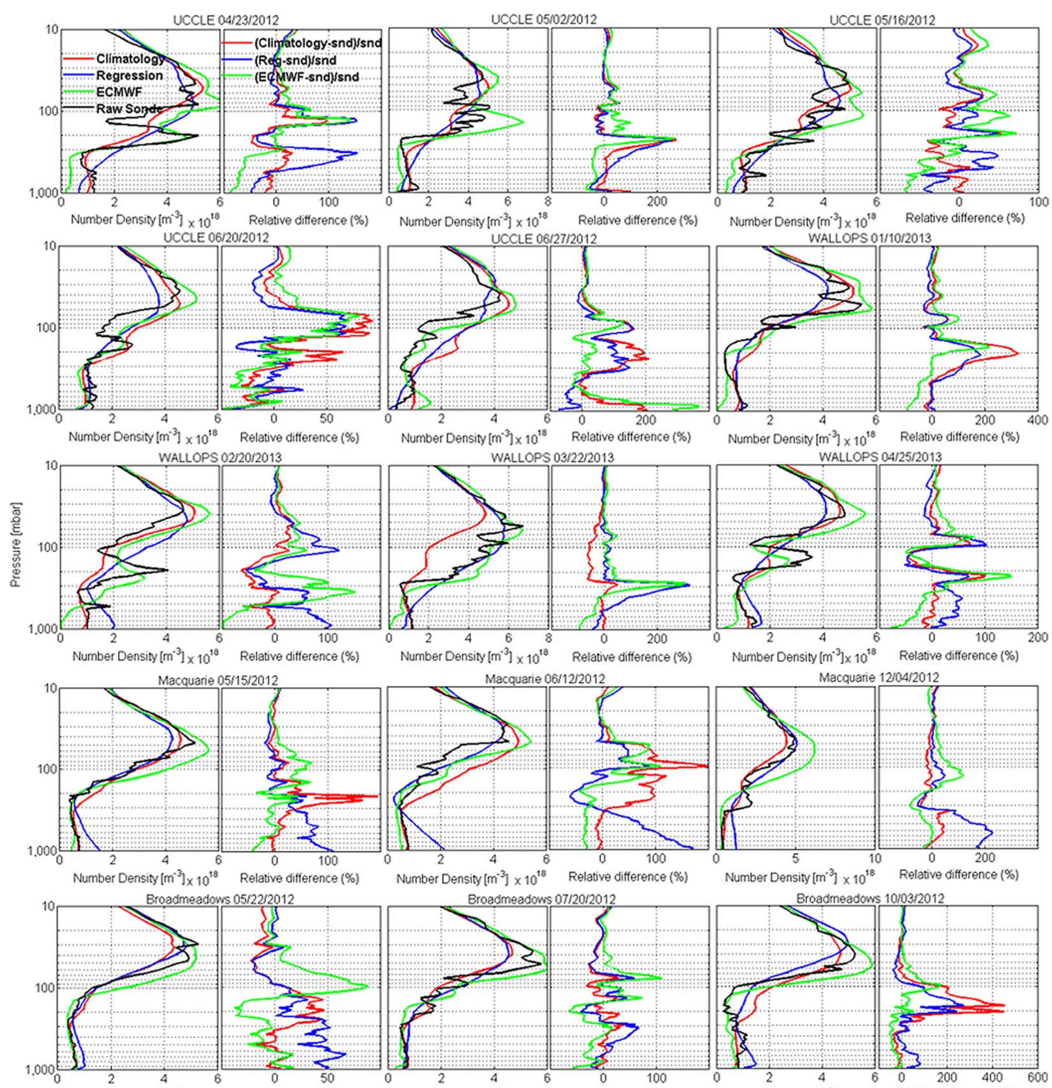

(b)

Fig. 3. Regression, ECMWF, and climatological ozone profiles compared with ozonesondes. The three plots show the comparison results from high latitude to low latitude in the Southern Hemisphere and the Northern Hemisphere, respectively. “snd” is the ozonesonde profile. (a) High latitudes. (b) Midlatitudes. (c) Tropics.

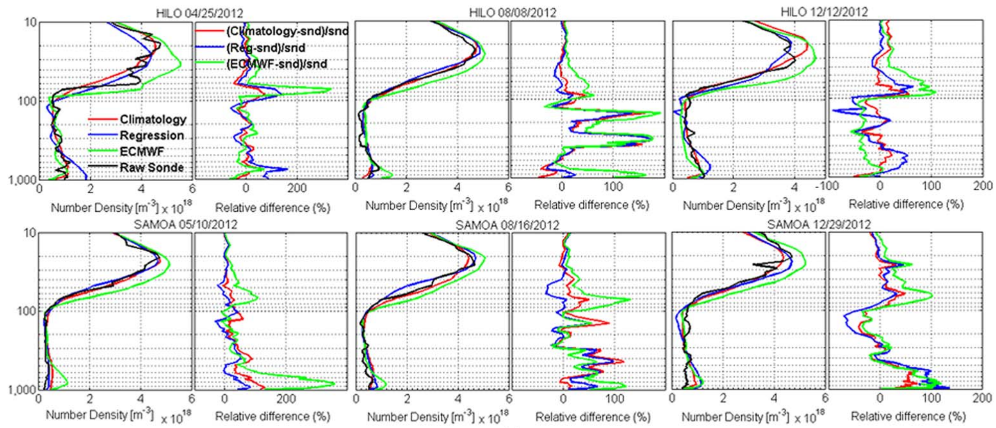

(c)

Fig. 3. (Continued) Regression, ECMWF, and climatological ozone profiles compared with ozonesondes. The three plots show the comparison results from high latitude to low latitude in the Southern Hemisphere and the Northern Hemisphere, respectively. "snd" is the ozonesonde profile. (a) High latitudes. (b) Midlatitudes. (c) Tropics.

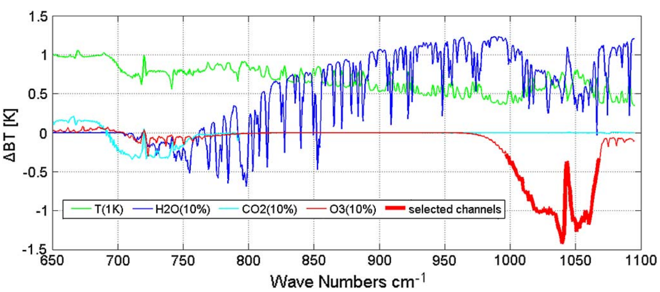

Fig. 4. Brightness temperature response between the reference and test spectra for a tropical air mass.

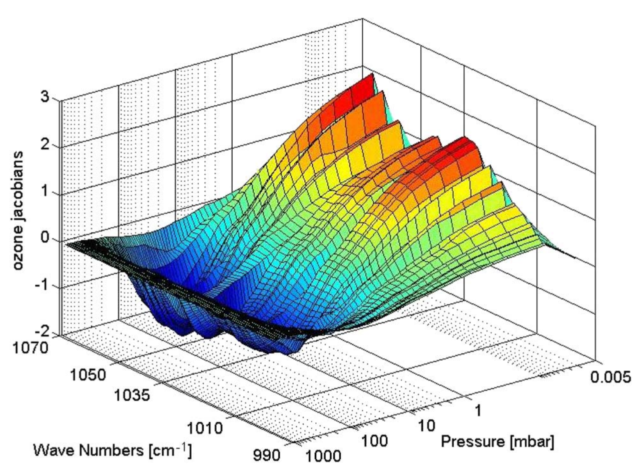

Fig. 5. Absolute values of the ozone Jacobian matrix at selected channels for a tropical air mass.

which represents the sensitivity of the retrieved $\hat{x}$ state to the true state x, i.e.,

$$A = \frac{d\hat{x}}{dx} = GK \tag{8}$$

where G is the gain matrix, which is defined as

$$G = \frac{\partial \hat{x}}{\partial y} = \left(K^T S_\varepsilon^{-1} K + S_a^{-1}\right)^{-1} K^T S_\varepsilon^{-1} = \hat{S} K^T S_\varepsilon^{-1} \tag{9}$$

where $\hat{S}$ is the solution error covariance matrix. The retrieved state can be related to the true state through

$$\hat{x} - x_a = G\left[K(x - x_a) + \varepsilon\right] = A(x - x_a) + G\varepsilon. \tag{10}$$

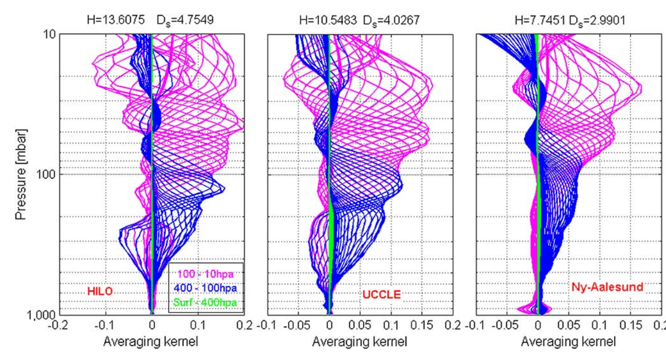

Fig. 6. Examples of AKs for the measurements over HILO, UCCLE, and Ny-Aalesund.

The degrees of freedom for a signal d_s and the Shannon information content H can be used to characterize the change in the knowledge of the state as a result of making a measurement. The parameter d_s represents the number of independent parameters that define the improvement of the retrieved profile over the *a priori*, and H is an overall measure of the signal-to-noise ratio relative to the *a priori* [32]. They are given by

$$H = \frac{1}{2} \sum_i \ln\left(1 + \lambda_i^2\right) \tag{11}$$

$$d_s = \sum_i \frac{\lambda_i^2}{(1 + \lambda_i^2)} \tag{12}$$

where λ_i is a singular value of $\tilde{K} = S_\varepsilon^{-1/2} K S_a^{1/2}$.

There are four types of errors: smoothing error S_s, forward model parameter error S_p, forward model error S_f, and retrieval random noise error S_m. The sum of S_m and S_s is $\hat{S}$, as shown in (9). The total error covariance S_{total} is the sum of the four error sources [32]. Thus

$$S_s = (A - I) S_a (A - I)^T \tag{13}$$

$$S_p = G K_b S_b K_b^T G^T \tag{14}$$

$$S_f = G \cdot \Delta F \tag{15}$$

$$S_m = G S_\varepsilon G^T \tag{16}$$

$$S_{\text{total}} = S_s + S_m + S_p + S_f. \tag{17}$$

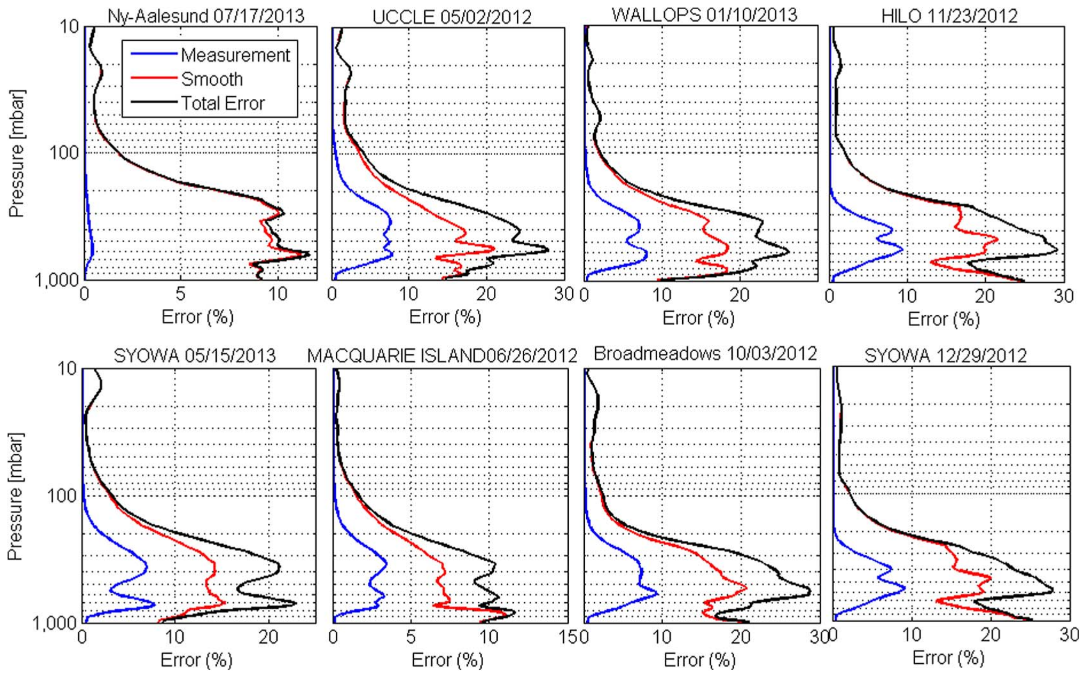

Fig. 7. Error analyses at eight of the sites. The errors are the square roots of the diagonal elements of the error covariance matrix.

IV. Results and Discussion

A. Characterization and Error Analysis of Retrievals

Fig. 6 shows the sample AK matrices for the CrIS observations over HILO, UCCLE, and Ny-Aalesund. AK matrices characterize the sensitivity of the retrieved profiles relative to the true state of the atmosphere. These three measurements show different sensitivities to the ozone vertical distribution. The analysis reveals that the CrIS sensitivity to the ozone profile is greatest in the stratosphere (100–10 hPa). The information content and the degree of freedom are low ($H = 7.7451$, $d_s = 2.9901$), medium ($H = 10.5483$, $d_s = 4.0267$), and high ($H = 13.6075$, $d_s = 4.7549$).

The error analyses in Fig. 7 show that the smoothing error exceeds the measurement error. The errors resulting from the simultaneous retrievals of surface properties (temperature and emissivity) and constituent concentrations such as H_2O and CO_2 are weak and are not shown. The total error varies from 0% to 30% for each individually retrieved level of the profile, and the total error is lower in the high latitudes and higher in the middle and low latitudes. The errors are highest in the surface to 400-hPa section because of tropopause variability.

B. Comparison With Ozonesonde Observations

The retrievals were validated with ozonesonde observations that were measured using electrochemical concentration cells (ECCs) that rely on the oxidation of a potassium iodide (KI) solution by the ozone in the ambient air. There retrievals are available from the World Ozone and Ultraviolet Data Center (WOUDC, http://www.woudc.org) archive. The accuracy of the ECC sondes is estimated to be approximately ±(5–10)% up to an altitude of 30 km, and the precision is estimated to be better than ±(3–5)%.

TABLE I
Summary of the Sounding Stations Used in This Study

Ozonesonde Station	Latitude °N	Longitude °E	Altitude m	Number of Sonde Data	Coincidences
SYOWA	-69.0	39.58	22.0	2	32
MACQUARIE ISLAND	-54.5	158.967	6.0	3	28
SAMOA	-14.25	-170.56	82.0	3	41
HILO	19.5735	-155.0485	11.0	3	37
WALLOPS	37.898	-75.483	13.0	4	48
Broadmeadows	-37.69	144.95	110.0	3	33
UCCLE	50.8	4.35	100.0	5	62
Ny-Aalesund	78.933	11.883	242.5	2	20

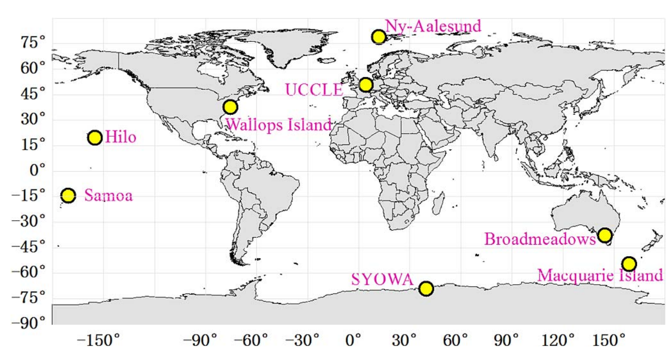

Fig. 8. Locations of the WOUDC stations used in this study.

The ozonesondes were matched to the CrIS retrievals using the following quality screening criteria: 1) within 100 km; 2) within 12 h; and 3) the CrIS measurement should involve a cloudless sky. Sample data sets between May 2012 and July 2013 were selected at eight stations ranging from the tropics to the polar regions. The stations are summarized in Table I, and the locations are shown in Fig. 8.

The sonde measurements provide vertical profiles between the surface and approximately 30–35 km. Because they have very high vertical resolutions, the profiles need to be smoothed

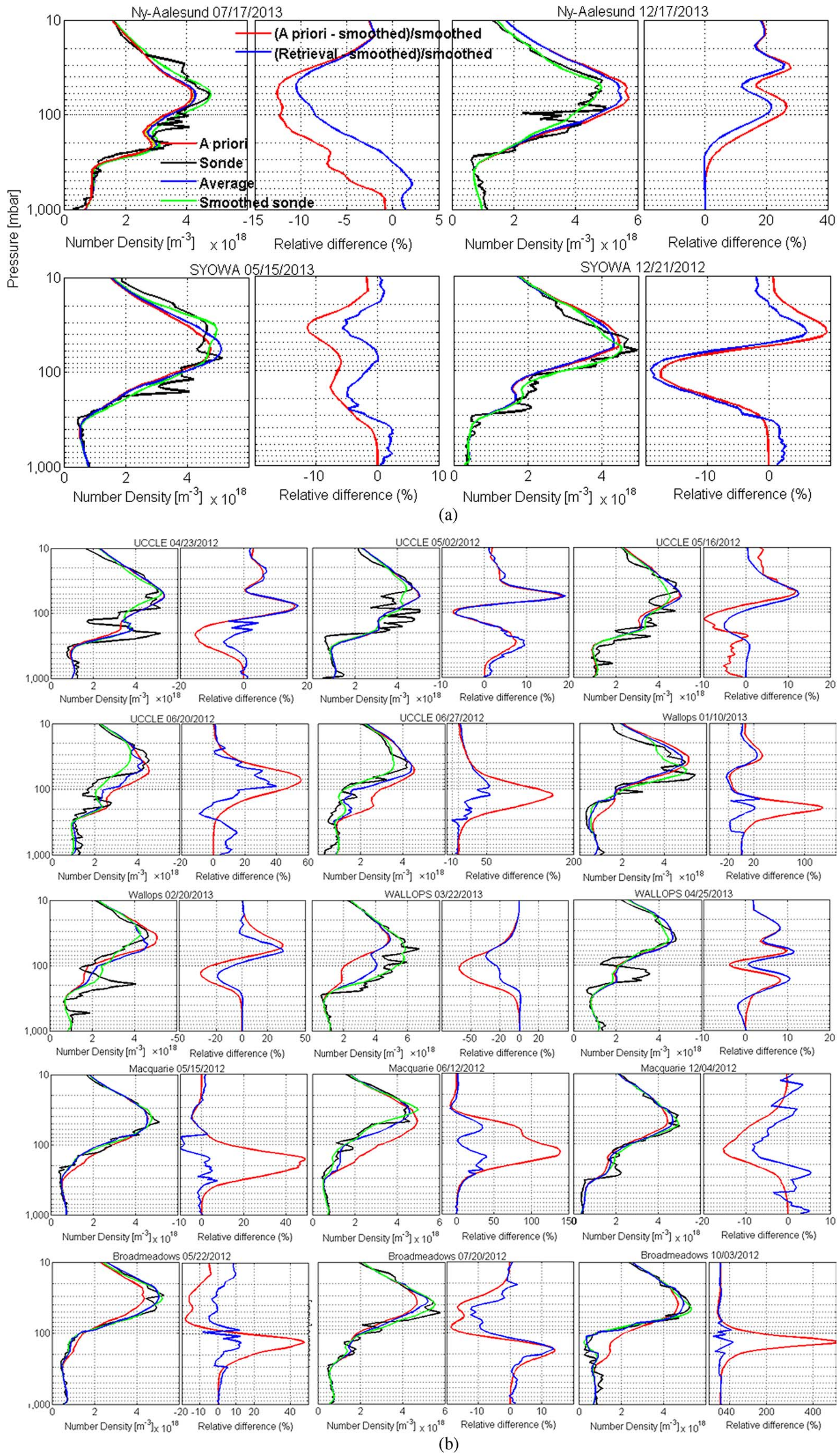

Fig. 9. Retrieved ozone profiles in number density units: (a) high latitudes, (b) middle latitudes, and (c) tropics. The relative differences were calculated with respect to the smoothed profile.

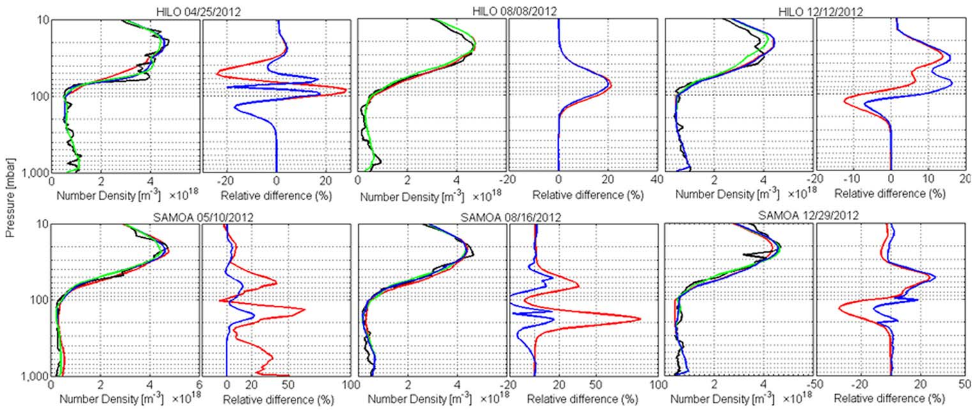

(c)

Fig. 9. (Continued) Retrieved ozone profiles in number density units: (a) high latitudes, (b) middle latitudes, and (c) tropics. The relative differences were calculated with respect to the smoothed profile.

according to the AK matrix of the CrIS retrievals in order to take into account the different vertical resolutions and to allow meaningful comparisons with the retrieved ozone profiles. We obtained the smoothed ozonesonde profiles using

$$x_s = Ax_{\text{sonde}} + (I - A)x_a \tag{18}$$

where I is the identity matrix, and x_{sonde} is the measured ozonesonde profile. In the ideal case, A would be an identity matrix, and x_s is the smoothed ozonesonde profile.

Fig. 9(a)–(c) shows the retrieval results for the high latitudes (Ny-Aalesund and SYOWA), midlatitudes (UCCLE, WALLOPS, MACQUARIE ISLAND, and Broadmeadows), and tropics (HILO and SAMOA) in the northern and Southern Hemispheres, respectively. The relative differences were calculated with respect to the smoothed profile. The colors of the profiles are as follows: *a priori* in red, retrieved CrIS profiles in blue, interpolated sonde in black, and AK-smoothed sonde in green. The colors of the relative differences are as follows: (*a priori*–smoothed sonde)/smoothed in red and (retrieval–smoothed sonde)/smoothed sonde in blue.

We plotted all of the match points at the Ny-Aalesund [STN89; see Fig. 9(a), left] site and then averaged all of the retrievals for comparison with the smoothed ozonesonde profile. At the other sites, we used the closest retrieval for the comparison. The retrieval results show good agreement with the smoothed profile. The precision is generally good in the stratosphere (better than 10% above 100 hPa), but is poor in the midlatitudes, where it reaches 20%. In the troposphere, the highest precision was 5% between the surface and 300 hPa, whereas in the 100- to 300-hPa layer, the precision was poor and reached 30%. The value of the AKs from the surface to 400 hPa is close to zero, and the calculated profiles, according to (18) are pulled toward the *a priori* profile below 400 hPa.

From the overall results, we found that the difference in the inversion precision between the hemispheres was not large and was better in the middle and high latitudes and poorer in the low latitudes. This pattern is due to the convolution. We do not have all of the information from the satellite, and we should therefore consider the negative side effects of convolution by the AKs, which can artificially improve the comparison [19].

V. Summary

In this paper, ozone vertical profile retrievals from a set of CrIS spectra between May 2012 and July 2013 have been presented. The retrieval algorithm was based on an optimal estimation technique, and the ozone climatology profile was used to construct the *a priori* state.

We compared the retrieved ozone profiles with coincident smoothed and convolved ozonesonde data at eight stations, and the retrieval results captured the ozone temporal and spatial variations well and showed good agreement with the smoothed profiles. The inversion errors were less than 10% in the stratosphere and less than 5% at the bottom of the troposphere, whereas large errors were present in the middle troposphere (30%). We also found that the information in the retrieved profiles was primarily from the *a priori* profile below 400 hPa.

This is the first step to an operational ozone product, and the results should be regarded as encouraging but preliminary. A radiative transfer model with high accuracy and better knowledge of the Earth's surface temperature, local emissivity, atmospheric temperature, and humidity profiles are also needed. Such improvements would improve the accuracy of the ozone satellite remote sensing retrievals, particularly for nadir viewing thermal sounding instruments. A future paper will look at how to improve the accuracy of those parameters by the eigenvector regression method.

Acknowledgment

The authors would like to thank the CrIS, WOUDC, and ERA-Interim Team for the data used in our work. They would also like to thank R. D. McPeters, who provided the ozone climatology, and the two anonymous reviewers for their assistance in evaluating this paper.

REFERENCES

[1] E. E. Borbas, S. W. Seemann, H.-L. Huang, J. Li, and W. P. Menzel, "2005: Global profile training database for satellite regression retrievals with estimates of skin temperature and emissivity," in *Proc. 14th Int. ATOVS Study Conf., Beijing, China, Univ. Wisconsin-Madison, Space Sci. Eng. Center, CIMSS*, Madison, WI, USA, 2005, pp. 763–770.

[2] H. Bovensmann *et al.*, "SCIAMACHY: Mission objectives and measurement modes," *J. Atmos. Sci.*, vol. 56, no. 2, pp. 127–150, 1999, doi:10.1175/1520-0469(1999)0560127:SMOAMM2.0.CO;2.

[3] A. Boynard *et al.*, "Measurements of total and tropospheric ozone from IASI: Comparison with correlative satellite, ground-based and ozonesonde observations," *Atmos. Chem. Phys.*, vol. 9, no. 16, pp. 6255–6271, 2009.

[4] J. P. Burrows *et al.*, "The Global Ozone Monitoring Experiment (GOME): Mission concept and first scientific results," *J. Atmos. Sci.*, vol. 56, no. 2, pp. 151–175, 1999.

[5] C. Carter, Q. Liu, W. Yang, D. Hommel, and W. Emery, "Neat heat flux, visible/infrared imager/radiometer suite algorithm theoretical basis document," Raytheon Nat. Polar-orbiting Observ. Satellite Syst. (NPOESS), Waltham, MA, USA, SBRS Doc. Y2407-NetHeatFlux-ATBD-Rev5. [Online]. Available: http://npoesslib.ipo.noaa.gov/u_listcategory_v3.php?35

[6] L. F. Chen *et al.*, "The couple-inversion of atmospheric profile and surface temperature and emissivity from MODIS data," in *Proc. IEEE IGARSS*, 2002, vol. 3, pp. 1630–1632.

[7] C. Clerbaux *et al.*, "Monitoring of atmospheric composition using the thermal infrared IASI/MetOp sounder," *Atmos. Chem. Phys.*, vol. 9, pp. 6041–6054, 2009, doi:10.5194/acp-9-6041-2009.

[8] P.-F. Coheur *et al.*, "Retrieval and characterization of ozone vertical profiles from a thermal infrared nadir sounder," *J. Geophys. Res.*, vol. 110, no. D24, Dec. 2005, Art. no. D24303, doi:10.1029/2005JD005845.

[9] D. P. Dee *et al.*, "The ERA-Interim reanalysis: Configuration and performance of the data assimilation system," *Q. J. R. Meteorol. Soc.*, vol. 137, no. 656, pp. 553–597, Apr. 2011, doi:10.1002/qj.828.

[10] M. Divakarla *et al.*, "Evaluation of Atmospheric Infrared Sounder ozone profiles and total ozone retrievals with matched ozonesonde measurements, ECMWF ozone data, and Ozone Monitoring Instrument retrievals," *J. Geophys. Res.*, vol. 113, no. D15, Aug. 2008, Art. no. D15308, doi:10.1029/2007JD009317.

[11] J. R. Eyre, "Inversion methods for satellite sounding data," in *Proc. ECMWF Meteorol. Train. Course Lect. Ser.*, 1991, pp. 1–20.

[12] L. E. Flynn *et al.*, "Measurements and products from the Solar Backscatter Ultraviolet (SBUV/2) and Ozone Mapping and Profiler Suite (OMPS) instruments," *Int. J. Remote Sens.*, vol. 30, pp. 4259–4272, 2009, doi:10.1080/01431160902825040.

[13] L. Flynn *et al.*, "Performance of the Ozone Mapping and Profiler Suite (OMPS) products," *J. Geophys. Res. Atmos.*, vol. 119, pp. 6181–6195, 2014, doi:10.1002/2013JD020467.

[14] R. J. Glumb, D. C. Jordan, and P. Mantica, "Development of the Crosstrack Infrared Sounder (CrIS) sensor design," in *Proc. Int. Symp. Opt. Sci. Technol. Int. Soc. Opt. Photon.*, 2002, pp. 411–424.

[15] Y. P. Han *et al.*, "JCSDA Community Radiative Transfer Model (CRTM)-Version1," National Oceanic and Atmospheric Administration (NOAA), Silver Spring, MA, USA, Tech. Rep. NESDIS 122, 2006.

[16] D. F. Heath, A. J. Krueger, H. R. Roeder, and B. D. Henderson, "The Solar Backscatter Ultraviolet and Total Ozone Mapping Spectrometer (SBUV/TOMS) for Nimbus G," *Opt. Eng.*, vol. 14, pp. 323–331, 1975.

[17] *IPCC Climate Change 2013: The Physical Science Basis*, T. F. Stocker *et al.*, Eds. New York, NY, USA: Cambridge Univ. Press, 2013. [Online]. Available: http://www.ipcc.ch/report/ar5/wg1/

[18] I. Petropavlovskikh, P. K. Bhartia, and J. DeLuisi, "An improved Umkehr algorithm," Nat. Ocean. Atmos. Admin. (NOAA) Coop. Inst. Res. Environ. Sci., 2004. [Online]. Available: http://www.srrb.noaa.gov/research/umkehr/append_umk_pdf.pdf

[19] C. Keim *et al.*, "Tropospheric ozone from IASI: Comparison of different inversion algorithms and validation with ozone sondes in the northern middle latitudes," *Atmos. Chem. Phys.*, vol. 9, no. 24, pp. 9329–9347, 2009.

[20] J. Lelieveld and F. J. Dentener, "What controls tropospheric ozone?" *J. Geophys. Res.*, vol. 105, pp. 3531–3551, 2000.

[21] X. Liu *et al.*, "Ozone profile and tropospheric ozone retrievals from the Global Ozone Monitoring Experiment: Algorithm description and validation," *J. Geophys. Res.*, vol. 110, 2005, Art. no. D20307, doi:10.1029/2005JD006240.

[22] M. Pengfei *et al.*, "Simulation of atmospheric temperature and moisture profiles retrieval from CrIS observations," *Spectrosc. Spectral Anal.*, vol. 34, no. 7, pp. 1894–1897, 2014.

[23] M. Pengfei *et al.*, "Simulation of atmospheric nitrous oxide profiles retrieval from AIRS observations," *Spectrosc. Spectral Anal.*, vol. 35, no. 6, pp. 1690–1694, 2015.

[24] R. D. McPeters *et al.*, Nimbus-7 Total Ozone Mapping Spectrometer (TOMS) Data Products User's Guide, 1996a, last access: Nov. 21, 2012. [Online]. Available: http://macuv.gsfc.nasa.gov/doc/n7usrguide.pdf

[25] R. D. McPeters, S. M. Hollandsworth, L. E. Flynn, J. R. Herman, and C. J. Seftor, "Long-term ozone trends derived from the 16 year combined Nimbus 7/Meteor 3 TOMS Version 7 record," *Geophys. Res. Lett.*, vol. 23, no. 25, pp. 3699–3702, 1996b, doi:10.1029/96GL03540.

[26] R. D. McPeters and G. J. Labow, "Climatology 2011: An MLS and sonde derived ozone climatology for satellite retrieval algorithms," *J. Geophys. Res.*, vol. 117, 2012, Art. no. D10303, doi:10.1029/2011JD017006.

[27] R. D. McPeters, P. K. Bhartia, D. Haffner, G. J. Labow, and L. Flynn, "The version 8.6 SBUV ozone data record: An overview," *J. Geophys. Res. Atmos.*, vol. 118, no. 14, pp. 8032–8039, 2013, doi:10.1002/jgrd.50597.

[28] N. R. Nalli, P. J. Minnett, and P. van Delst, "Emissivity and reflection model for calculating unpolarized isotropic water surface-leaving radiance in the infrared. 1: Theoretical development and calculations," *Appl. Opt.*, vol. 47, no. 21, pp. 3701–3721, 2008.

[29] R. Nassar *et al.*, "Validation of Tropospheric Emission Spectrometer (TES) nadir ozone profiles using ozonesonde measurements," *J. Geophys. Res.*, vol. 113, 2008, Art. no. D15S17, doi:10.1029/2007JD008819.

[30] V. Natraj *et al.*, "Multi-spectral sensitivity studies for the retrieval of tropospheric and lowermost tropospheric ozone from simulated clear-sky geo-cape measurements," *Atmos. Environ.*, vol. 45, no. 39, pp. 7151–7165, 2011.

[31] C. D. Rodgers, "Characterization and error analysis of profiles retrieved from remote sounding measurements," *J. Geophys. Res.*, vol. 95, no. D5, pp. 5587–5595, 1990.

[32] C. D. Rodgers, *Inverse Methods for Atmospheric Sounding: Theory and Practice*. Singapore: World Scientific, 2000.

[33] C. D. Rodgers and B. J. Connor, "Intercomparison of remote sounding instruments," *J. Geophys. Res.*, vol. 108, no. D3, p. 4116, Feb. 2003.

[34] H. G. J. Smit *et al.*, "Assessment of the performance of ECC-ozonesondes under quasi-flight conditions in the environmental simulation chamber: Insights from the Juelich Ozone Sonde Intercomparison Experiment (JOSIE)," *J. Geophys. Res.*, vol. 112, 2007, Art. no. D19306, doi:10.1029/2006JD007308.

[35] W. L. Smith and H. M. Woolf, "The use of eigenvectors of statistical covariance matrices for interpreting satellite sounding radiometer observations," *J. Atmos. Sci.*, vol. 33, no. 7, pp. 1127–1140, 1976.

[39] W. L. Smith *et al.*, "Dual-regression retrieval algorithm for real-time processing of satellite ultraspectral radiances," *J. Appl. Meteorol. Climatol.*, vol. 51, no. 8, pp. 1455–1476, 2012.

[37] J. M. Wallace and P. V. Hobbs, *Atmospheric Science: An Introductory Survey*. New York, NY, USA: Academic, 2006.

[38] H. M. Worden *et al.*, "Comparisons of Tropospheric Emission Spectrometer (TES) ozone profiles to ozonesondes: Methods and initial results," *J. Geophys. Res.*, vol. 112, no. D3, Feb. 2007, Art. no. D03309, doi:10.1029/2006JD007258.

[39] P. F. Levelt *et al.*, "Science objectives of the ozone monitoring instrument," *IEEE Trans. Geosci. Remote Sens.*, vol. 44, no. 5, pp. 1199–1208, May 2012, DOI:10.1109/TGRS.2006.872336.

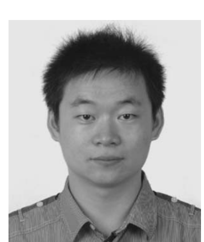

Pengfei Ma received the Ph.D. degree in cartography and geographical information system from the Institute of Remote Sensing and Digital Earth, Chinese Academy of Sciences, Beijing, China, in 2014.

He is currently an Intermediate Engineer of environmental remote sensing with the Satellite Environment Center, Ministry of Environmental Protection, Beijing. His research interests mainly focus on atmospheric trace gas retrieval.

Liangfu Chen received the Ph.D. degree in geography from Peking University, Beijing, China, in 1999.

He is currently a Professor with the Institute of Remote Sensing Applications, Chinese Academy of Sciences, Beijing. Since 2004, he has led an 863 project of China, "multi-source satellite remote sensing technology of atmospheric pollution monitoring," and the Knowledge Innovation Program of the Chinese Academy of Sciences. His research includes the retrieval and application of atmosphere aerosol and trace gases based on remote sensing data.

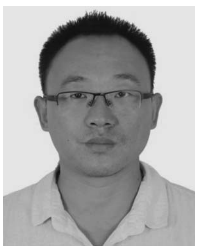

Zhongting Wang received the Ph.D. degree in cartography and geographical information system from the Institute of Remote Sensing Applications, Chinese Academy of Sciences, Beijing, China, in 2008.

He is currently a Senior Engineer of environmental remote sensing with the Satellite Environment Center, Ministry of Environmental Protection, Beijing. For the past ten years, his primary research interest has been in atmospheric model simulations and atmospheric remote sensing.

Shaohua Zhao received the Ph.D. degree in physical geography from Beijing Normal University, Beijing, China, in 2008.

From 2008 to 2010, he engaged in postdoctoral research at Peking University, Beijing. He is currently a Senior Engineer with the Satellite Environment Center, Ministry of Environmental Protection, Beijing. His research interests focus on the remote sensing of environment, and he has authored or coauthored over 70 related papers.

Qing Li received the Ph.D. degree in geodetection and information technology from the China University of Geosciences, Hubei, China, in 2002.

She is currently a Professor with the Satellite Environment Center, Ministry of Environmental Protection, Beijing, China. In recent years, she has taken part in some national key projects concerning satellite remote sensing, such as National 863 project (Research on software platform and operational demonstration application for environmental remote sensing monitoring) and National key basement research 973 project (Research on comprehensive multi-scale aerosol observation and its temporal and spatial distribution characteristics). She is currently leading a group to do air quality monitoring and relevant comprehensive evaluation research work based on remote sensing technology. Her research includes environmental remote sensing and applications.

Minghui Tao received the Ph.D. degree in atmospheric science from the Institute of Remote Sensing and Digital Earth, Chinese Academy of Sciences, Beijing, China, in 2013.

He is currently a Research Associate with the Institute of Remote Sensing and Digital Earth. His research focus is on the formation mechanism and climate effects of regional air pollution in China with A-Train satellite observations and ground measurements.

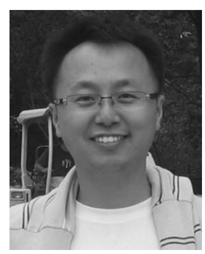

Zifeng Wang received the Bachelor's degree from Peking University, Beijing, China, in 2005 and the D.Sc. degree from the Graduate University of Chinese Academy of Sciences, Beijing, in 2010.

He is currently an Associate Professor with the Institute of Remote Sensing and Digital Earth, Chinese Academy of Sciences, Beijing. His research interests mainly focus on the following: 1) satellite estimation of the ground-level particulate matters; 2) comprehensive analysis of haze pollution using multiple remote sensing; and 3) spatial and temporal trend analysis of regional air quality using space observations.